Experimental evaluation of a flapping-wing aerodynamic model for MAV applications

Jun-Seong Lee[a], Dae-Kwan Kim[b], Jin-Young Lee[a], Jae-Hung Han[a]

[a] Department of Aerospace Engineering, KAIST,
335 Gwahangno, Yuseong-gu, Daejeon, 305-701, Republic of Korea
[b] COMS Systems Department, Communication, Ocean & Meteorological Satellite Program Office,
Korea Aerospace Research Institute, Daejeon, 305-333, Republic of Korea

< Article Info. >

Publication Title	**SPIE 15th Annual Symposium Smart Structures and Materials**
Journal Homepage	http://spie.org/
Publication Year	**2008**
Volume/Issue	**Vol.6928, 69282M**
Paginations	
DOI	http://dx.doi.org/10.1117/12.776169
Further Info.	http://sss.kaist.ac.kr/
Remark	**This PDF file is based on the final submission to the publisher, and there might be slight change from the final form provided by the publisher.**

Experimental evaluation of a flapping-wing aerodynamic model for MAV applications

Jun-Seong Lee[a], Dae-Kwan Kim[b], Jin-Young Lee[a], Jae-Hung Han*[a]

[a] Department of Aerospace Engineering, KAIST,
335 Gwahangno, Yuseong-gu, Daejeon, 305-701, Republic of Korea

[b] COMS Systems Department, Communication, Ocean & Meteorological Satellite Program Office,
Korea Aerospace Research Institute, Daejeon, 305-333, Republic of Korea

ABSTRACT

In the preliminary design phase of the bio-inspired flapping-wing MAV (micro air vehicle), it is necessary to predict the aerodynamic forces around the flapping-wing under flapping-wing motion at cruising flight. In this study, the efficient quasi-steady flapping-wing aerodynamic model for MAV application is explained and it is experimentally verified. The flapping-wing motion is decoupled to the plunging and pitching motion, and the plunging-pitching motion generator with load cell assembly is developed. The compensation of inertial forces from the measured lift and thrust is studied to measure the pure aerodynamic loads on the flapping-wing. Advanced ratio is introduced to evaluate the unsteadiness of the flow and to make an application range of flapping-wing aerodynamic model.

Keywords: Bio-inspired, Flapping-wing, Aerodynamic model, Micro air vehicle, Wind tunnel testing, Advanced ratio

1. INTRODUCTION

The design of wing structures of flapping-wing vehicles is quite different from that in fixed- and rotary-wing aircraft. One of differences is the use of aeroelastic deformation. For the conventional aircrafts aeroelastic phenomena have been regarded as something to be avoided or prevented in general. However, for birds and insects, it is not always necessary to reduce or suppress those deformations because they indeed use the aeroelastic characteristics of their wing structures. Actually most of birds and bats can change their wing shapes actively to generate proper aerodynamic loads. However, it seems that the passive pitching caused by the interaction of flexible wing structures and aerodynamic loads contributes a lot to the increase in aerodynamic performances. The characteristics of flapping-wing aerodynamics are dependent upon the kinematics of wing motion, wing geometry, wing structural properties and flow condition. The flapping-wing aerodynamics governed by unsteady low Reynolds number flow has not been fully understood; especially the roles or effects of leading-edge vortex, span-wise flow, and delayed stall need to be further investigated. Currently, many researchers demonstrate their bio-inspired flapping-wing MAV by "trial-and-error" approaches.

Like a pigeon or magpie, bird-scale nature's flyers have higher aspect ratio wing, lower flapping frequency and relatively small wing deformation than insects or hummingbirds. Those creatures experience the quasi-steady flow field which is much more predictable than unsteady one. DeLaurier [1] established a flapping-wing aerodynamic model, called modified strip theory (MST). The aerodynamic model makes it possible to estimate the aerodynamic performances of bird-scale flapping-wing MAV in the phase of preliminary design and development. Kim [2] improved the MST to consider higher resultant angle of attack, and added the dynamic stall model for not only pitching but also plunging motion. He obtained the aerodynamic parameters used in MST from the steady state wind tunnel test data.

Even the flapping-wing aerodynamic model is very efficient analyzing tool but it should be validated by the refined experimental data under various kinematical and aerodynamic conditions. However, there are not enough experimental results at low Reynolds number regime and in the broaden range of wing kinematics parameters. Accordingly we developed an experimental device to acquire the aerodynamic data under various flapping-wing motions at low Reynolds numbers, and the experimental results were compared with MST simulation results.

* jaehunghan@kaist.ac.kr; phone +82-42-869-3723; fax +82-42-869-3710; http://sss.kaist.ac.kr

Active and Passive Smart Structures and Integrated Systems 2008, edited by Mehdi Ahmadian
Proc. of SPIE Vol. 6928, 69282M, (2008) · 0277-786X/08/$18 · doi: 10.1117/12.776169

2. EXPERIMENTAL SET-UP AND METHODS

To analyze the aerodynamic characteristics of the flapping-wing, we decoupled the flapping-wing motion into two mainly effective wing motions: plunging and pitching. Sunada et al. [3] developed a plunging and pitching motion generator; however they did the experiments in the water tank at very low actuation frequency. Okamoto et al. [4] also tried to measure the aerodynamic forces and moments around flat-plate wing under unsteady wing motions in the wind tunnel. But those experimental devices have some limitations such as small amplitudes (~0.5c) and low actuation frequency level (~1Hz). Birds have plunging amplitudes more than 2 times of their wing chord length. Flapping frequency depends on the wing span but they usually have 3~7Hz for 60cm wing span (*c.f.* Magpie) [7]. Considering nature's flapping motions, we developed relatively large amplitude (peak-to-peak 16cm) and high frequency (~10Hz) motion generator.

2.1 Plunging-pitching motion generator

Fig. 1 shows the overall shape of the developed plunging-pitching motion generator, consisting mainly of plunging motion generator, pitching motion generator and load cell assembly. Basically the scotch-yoke mechanism converts the rotational motion of the motor into the sinusoidal motion, and the attached balanced mass reduces the vibration of the entire system. The plunging frequency increases linearly with the speed of the plunging actuation motor and the speed is controlled by the external analog signal of inverter. Load cell assembly is attached to the plunging motion generator as shown in Fig. 2. It consists of two load cells (KTOYO-651AQ-3, 5kgf) to gauge the lift and the thrust directional forces, and connected to two dynamic strain amplifiers (DN-AM310). This part is hided in the aluminum fairing for the wind tunnel testing. The pitching motion generator is mounted on the lift directional load cell. And it can be replaced by three types of test bed, (1) static test jig to fix the angle of attack for steady state wind tunnel test of the test wing and the plunging-only test, (2) passive test jig to generate the passive pitching motion by translational spring as shown in Fig. 1 and (3) active test jig to install the stepping motor for active pitching control, respectively. In this paper, we used the static test jig to perform the steady state wind tunnel test and plunging motion only test at fixed angle of attack as an initial study of this research.

We used two long range displacement laser sensors (LB-301/LB-1201) to monitor the plunging and pitching wing motions. Before we installed the motion generator to the wind tunnel facility, we evaluated it by FFT data whether it generates proper motions of desired amplitudes and frequencies. Moreover, to find the relationship between [gf] and [mV], each directional load cell was calibrated by the weight of a balance. This experimental device needs 5 A/D ports (2 load cells-lift/thrust, 2 laser displacement sensors-plunging/pitching, 1 accelerometer-plunging) and 2 D/A ports (plunging frequency and wind tunnel speed control). All the signals are managed by RTI (Real-Time-Interface) DSP board (dSPACE-DS1103). The sampling time is fixed to 1ms throughout the experiment.

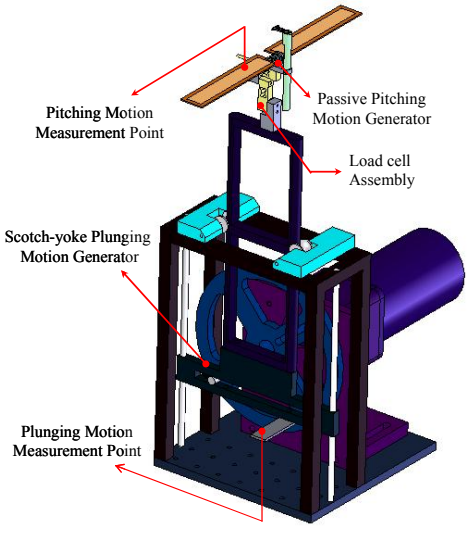

Fig 1 Plunging-pitching motion generator

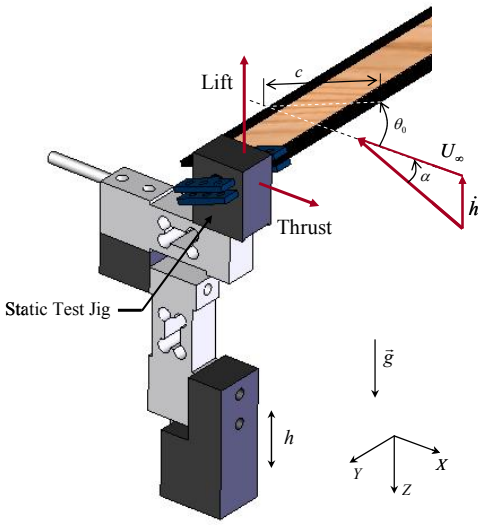

Fig 2 Load cell assembly and the direction of forces

The low pass filter with the cut-off frequency of 2.5 times of the plunging actuation frequency was applied to the entire sensor signals. The discrete Fourier transform filter was used to prevent the phase delay.

2.2 Inertial force modeling

The load cells attached to the plunging motion generator experience the acceleration of plunging motion. Due to the mass of load cell itself, we can observe the signal, but it can not be determined theoretically. To extract the pure aerodynamic loads from the combined signal of the inertia and the aerodynamic forces, we introduced the dynamic calibration of the load cell to make an inertial model.

First of all, we examined the structural characteristics of our measurement system by the modal test (PCB086C01, HP356xa). The first natural frequency of the experimental device is greater than 200Hz. The plunging motion actuation frequency f is adjusted from i=1Hz to 10Hz. Hence, we made sure that the change of structural properties of load cell assembly such as phase delay, and equivalent mass of load cell are not varied with the frequency.

The raw data of each load cell are composed of

$$F^L_{f=i} = \left(F^L_{f=i}\right)_I + \left(F^L_{f=i}\right)_A, \qquad F^T_{f=i} = \left(F^T_{f=i}\right)_I + \left(F^T_{f=i}\right)_A \tag{1}$$

The subscript I and A imply inertia and aerodynamic forces, and the superscript L and T denote lift and thrust, respectively. If there is no pitching motion generator which is mounted on the lift directional load cell, we could introduce the equivalent mass of load cell assembly m^L_e and m^T_e to build an inertial model of each direction.

$$\left(F^L_{f=i}\right)_{I,0} = m^L_e \cdot a^L_{f=i}, \qquad \left(F^T_{f=i}\right)_{I,0} = m^T_e \cdot a^T_{f=i} \tag{2}$$

In case the lift and the thrust directional accelerations are known, we can determine the equivalent mass.

$$m^L_e\Big|_{f=i} = \frac{\left\langle \left(F^L_{f=i}\right)_{I,0} \right\rangle_{RMS}}{\left\langle a^L_{f=i} \right\rangle_{RMS}}, \qquad m^T_e\Big|_{f=i} = \frac{\left\langle \left(F^T_{f=i}\right)_{I,0} \right\rangle_{RMS}}{\left\langle a^T_{f=i} \right\rangle_{RMS}} \tag{3}$$

The lift directional acceleration $a^L_{f=i}$ is easily calculated because the plunging motion has the exact sinusoidal form. In contrast, the thrust directional acceleration $a^T_{f=i}$ can not be derived simply. Hence we make the two dummy mass which have the different weights (m_{d1}=8.98g, m_{d2}=43.05g) and it can be assembled on the lift directional load cell just like the static test jig in Fig 2. When the dummy masses are installed, then the inertia forces can be expressed as

$$\left(F^L_{f=i}\right)_{I,dj} = (m^L_e + m_{dj}) \cdot \left(a^L_{f=i}\right)_{dj}, \qquad \left(F^T_{f=i}\right)_{I,dj} = (m^L_e + m_{dj}) \cdot \left(a^T_{f=i}\right)_{dj} \tag{4}$$

From equations (2) and (4), we can get the acceleration components as follows:

$$\left(a^L_{f=i}\right)_{dj} = \frac{\left(F^L_{f=i}\right)_{I,dj} - \left(F^L_{f=i}\right)_{I,0}}{m_{dj}}, \qquad \left(a^T_{f=i}\right)_{dj} = \frac{\left(F^T_{f=i}\right)_{I,dj} - \left(F^T_{f=i}\right)_{I,0}}{m_{dj}} \tag{5}$$

Finally we averaged those acceleration values to get much precise ones. Based on the result of the equation (5), we can express them to analytical forms.

$$a^L_{f=i}(t) = -h(2\pi f)^2 \sin(2\pi f t), \quad a^T_{f=i}(t) = C_1 \cdot h(2\pi f)^2 \left(\sin(2\pi f t) + (1 + C_2)\sin(2\pi (2f) t + \pi)\right) \tag{6}$$

where C_1=0.01889, $C_2 \approx 0.0$ for $i = 1$ to 9.

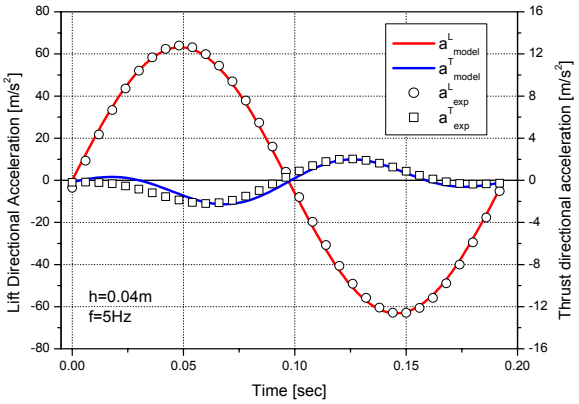

Fig 3 Lift and thrust directional acceleration modeling

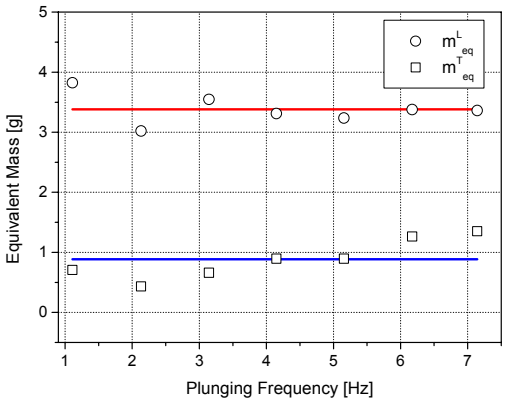

Fig 4 Equivalent mass of lift and thrust direction

The coefficients C_1 and C_2 represent the structural coupling factor between the lift and the thrust. It is determined by the curve fitting to minimize the error between the experiment data (5) and the acceleration model (6) for i=1 to 9. Fig 3 represents the result of the lift and the thrust directional accelerations modeling at h=0.04m and f=5Hz.

From the equation (3), the equivalent masses of each directional load cell can be evaluated as shown in Fig 4. It is confirmed that the equivalent masses are not varied with the actuation frequency, and that they have the mean values of m_e^L=3.3829g and m_e^T=0.8870g with the standard deviation 0.25g and 0.33g, respectively.

Adding the inertial effects of static or passive test jig, we can calculate the total inertial forces. Eventually we can separate the signal from the inertia combined one to pure aerodynamic loads.

$$\left(F_{f=i}^L\right)_I = (m_e^L + m_{test} + m_w^*)\cdot a_{f=i}^L, \qquad \left(F_{f=i}^T\right)_I = (m_e^T + m_{test} + m_w^*)\cdot a_{f=i}^T$$

$$\text{where } m_{test,static} = m_{d1},\ m_{test,dynamic} = m_{d2},\ m_w^* = m_w + m_{jo\,\text{int}} = 15.37\text{g} \qquad (7)$$

2.3 Wind tunnel tests of the plunging-pitching motion

Fig. 5 shows the experimental device assembled to the low-speed wind tunnel facility in KAIST. The wind tunnel has 30 x 30cm square and 100cm length test section, and the flow velocity can be controlled from 1m/s to 15m/s.

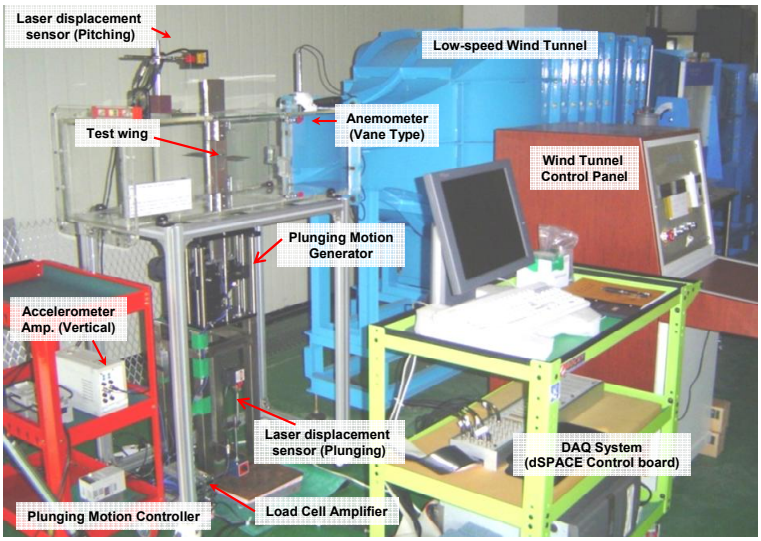

Fig 5 Plunging-pitching motion generator installed in the low-speed wind tunnel

To use our flapping-wing aerodynamic model, MST, we started the wind tunnel testing to get the static lift and drag coefficients versus angle of attack of the test wing that has the span b =180mm, chord length c =30mm, thickness t =1.5mm, aspect ratio AR =6 and mass m_w =7.45g. It is made of carbon/epoxy frame and balsa to resist the aerodynamic forces and it is sufficiently rigid in the range of 1~10Hz excitation frequency. We simulated our aerodynamic model at zero frequency to get the aerodynamic parameters which have the least error compared with the experiment data of the steady state wind tunnel testing of the airfoil. Then using these parameters, summarized in Equation (8), we could estimate the aerodynamic forces induced by dynamic plunging and pitching motion without further experiments.

As shown in the Fig 6, the angle of attack was adjusted from -20 deg to 20 deg with 2 deg increments at the flow velocities U_∞ = 6 and 8m/s, Re =12400 and 16500, respectively.

$$\eta_s = 0.19,\ \left(C_d\right)_c^{upper} = 2.36,\ \left(C_d\right)_c^{lower} = 3.09,\ \left(C_d\right)_f = 0.09,$$
$$\alpha_{L0} = 0°,\ \left(\alpha_{stall}\right)_{\max} = 8.22°,\ \left(\alpha_{stall}\right)_{\min} = -8.82° \tag{8}$$

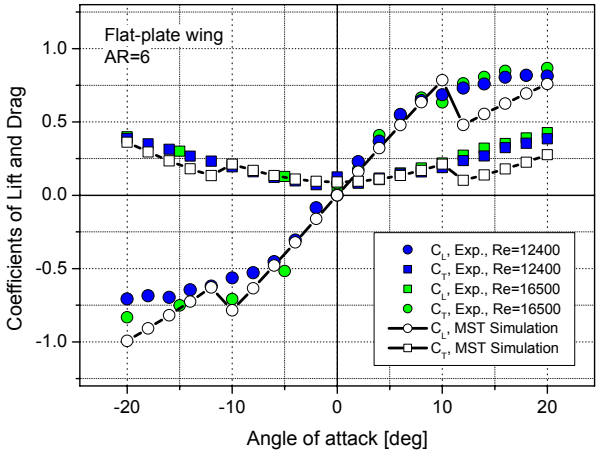

Fig 6 Lift and thrust coefficients at Re=12400 and Re=16500 with MST simulation results

2.4 Flapping-wing aerodynamic model, MST

DeLaurier [1] proposed the flapping-wing aerodynamic model by using simple strip theory. Mainly, this theory is evolved from the modification of the flutter analysis for large amplitude wing motion and low speed flow. Modified strip theory has the several assumptions: invariable finite span, continuous sinusoidal wing motion, and low resultant angle of attack. Various aerodynamic effects, such as camber effect, partial leading edge suction effect, viscous effect, unsteady wake effect, and dynamic stall model of pitching motion can be considered in this model. Kim [2] improved this aerodynamic model for the higher resultant angle of attack, and applied the dynamic stall model not only for the pitching but also plunging wing motion. This paper is focused on the experimental verification of our flapping-wing aerodynamic models ('MST' is original version [1] and 'MST-stall' is improved one [2]).

3. RESULTS AND DISCUSSION

Using the experimental set-up and methods described in the previous chapter, now the experimental data and the simulation results are analyzed. The experimental conditions in this paper are flow speed U_∞ =6m/s, plunging amplitude h =0.04m, plunging frequency f =1~9Hz (1Hz inc.) and fixed angle of attack θ_0 =0, 4, and 10 deg.

Shown Fig 7 is the time history of plunging motion, angle of attack, and lift and thrust coefficients at fixed angle of attack of 4 deg and the plunging frequency of 5Hz. 'MST-stall' and experiment data are very close but 'MST' can not

follow the value near the peak of lift coefficient. It addresses that the dynamic stall model and the stall criterion of MST-stall are better than those of 'MST'. The thrust coefficient of 'MST' is different with that of experimental result and 'MST-stall'. From the stall criterion used for 'MST', there is a big discontinuity during the upstroke. It produces the signal having the twice frequency, because we applied the numerical filter to make the same signal processing condition as the experimental data.

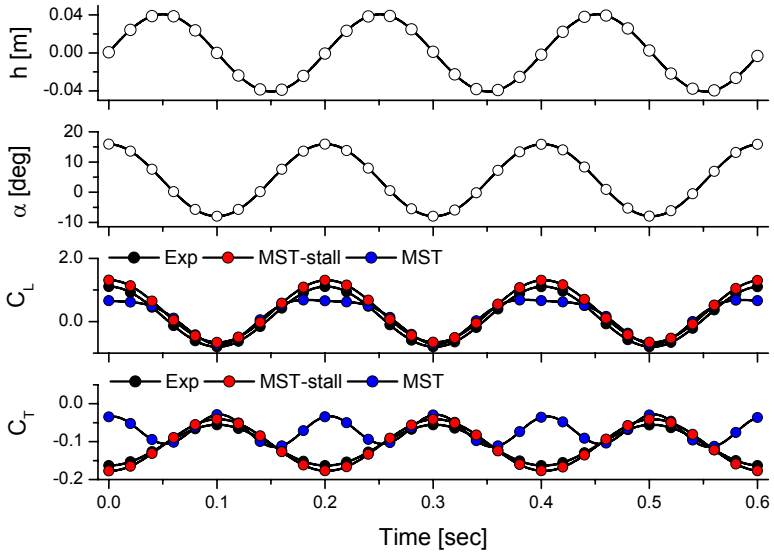

Fig 7 Time history of plunging-only test, U_∞ = 6m/s, θ_0 = 4°, f = 5Hz

The effective way to validate the aerodynamic model is to compare the mean and RMS (Root Mean Square) values of lift and thrust coefficients. The Figs. 8 and 9 show that the 'MST-stall' is better than 'MST' with better comparison with the experimental data over 5Hz. Even though there is no pitching motion; the dynamic stall model with MST-stall criterion calculates the accurate aerodynamic loads around the test wing.

The resultant angle of attack γ is calculated from the wing kinematical parameters [2]. So, the γ is increased with the increase in the plunging amplitude, plunging frequency and fixed mean angle of attack θ_0 at free stream velocity U_∞.

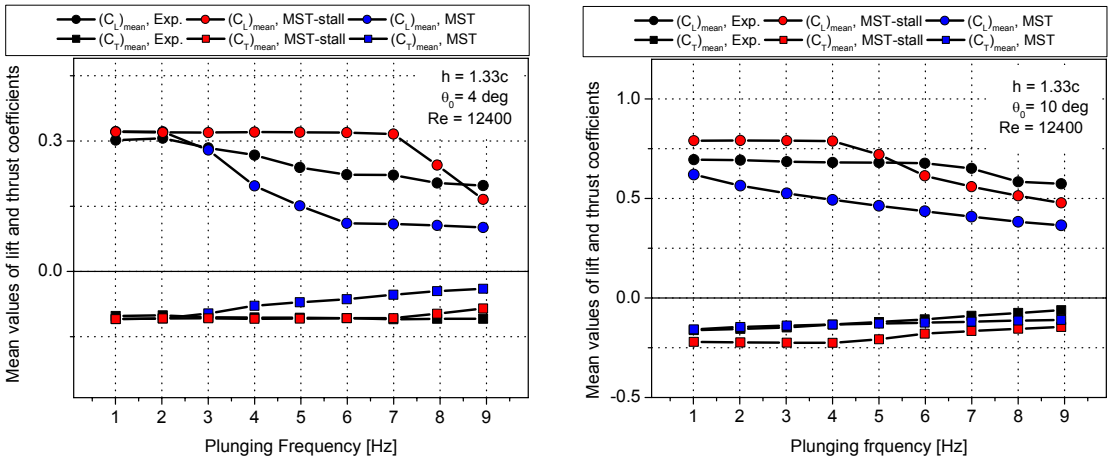

Fig 8 Mean lift and thrust coefficients h =0.04m, θ_0 =4 and 10°, Re =12400

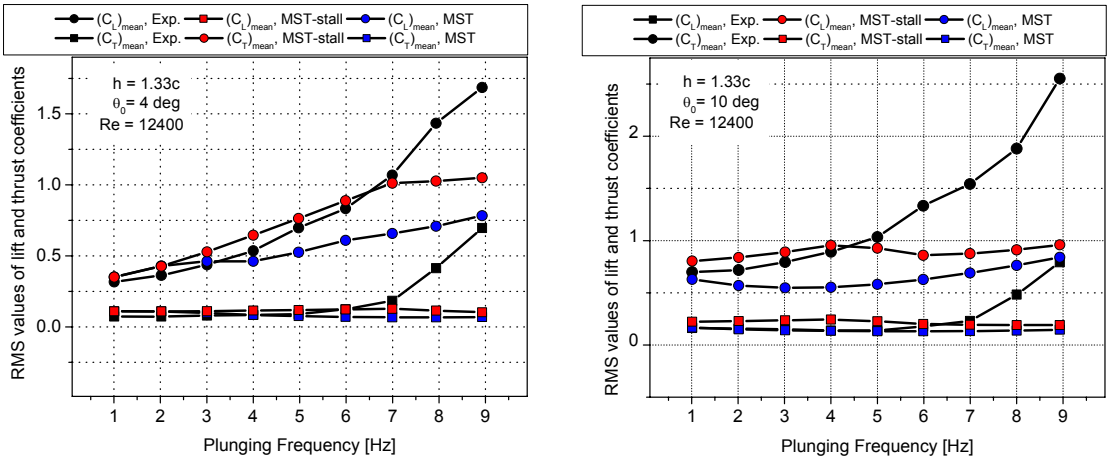

Fig 9 RMS lift and thrust coefficients h =0.04m, θ_0 =4 and 10°, Re =12400

The experimental conditions of Figs. 8 and 9 are the same except the fixed mean angle of attack θ_0. So, the fixed angle of attack directly affects the stall criterion. For the case θ_0 =4° in Fig 9, the RMS value of lift coefficient of 'MST-stall' starts to show discrepancy from the experimental data over the 6Hz. In addition the mean thrust coefficients have all negative values; the plunging-only test with fixed angle of attack could not make the positive mean value. The fixed angle of attack without pitching motion cases directly accelerates the stall phenomenon of test wing. However the wing of almost nature's flyers is flexible. It deforms passively or actively their pitching angle during the flapping motion to prevent or delay the stall phenomena. It is enough to use the 'MST-stall' to calculate the aerodynamic forces of the birds at the cruising flight condition.

Instead of monitoring the resultant angle of attack, we introduce the advance ratio J to judge the applicable range of MST. The MST is actually based on the quasi-steady flow regime; we can not apply it to the unsteady region. The unsteadiness of flapping-wing motion can be expressed as a dimensionless parameter, the advance ratio J. It is originally defined by the ratio of the flight speed to the speed of the wing tip for rotor blade. The smaller value of J has larger unsteadiness of the flow filed. In this research, the advance ratio is defined as $J = U_\infty / \dot{h} = U_\infty / h\omega$.

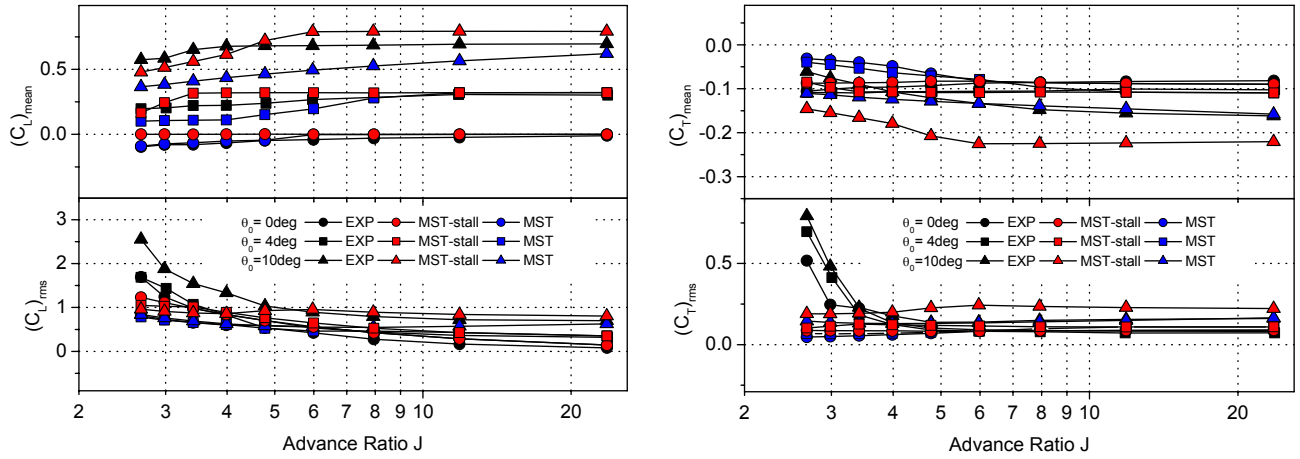

Fig 10 $\left(C_L\right)_{mean}$, $\left(C_L\right)_{rms}$, $\left(C_T\right)_{mean}$ and $\left(C_T\right)_{rms}$ Vs. Advance Ratio J at θ_0 =0, 4, 10°

The mean and RMS value of lift and thrust coefficients in Figs 8 and 9 are represented again by changing the x-axis from frequency to advance ratio. We found that our experimental conditions belonged to the region of the quasi-steady flow. However the advance ratio is smaller, the experimental data of lift and thrust coefficients are apparently increased but the MST simulation results could not follow up. Due to the fixed angle of attack, it associates frequently to the post-stall criterion and it contributes not only to enlarge the mean lift coefficients but also to drop the mean thrust coefficients.

4. CONCLUSIONS

We developed the plunging-pitching motion generator to measure the aerodynamic characteristics of unsteady wing motions at low Reynolds number flow. The dynamic calibration method of load cell assembly is introduced. Even though the acceleration information was not available, it was successful to build the inertial model of each directional load cell. The aerodynamic loads experimentally measured are compared with the simulation data of 'MST' and 'MST-stall'. The stall criterion using the higher resultant angle of attack was experimentally validated in the range of h=0.04m, θ_0=0, 4, 10 deg, f=1 to 9Hz. Finally we replaced the frequency to the advance ratio to find the applicable range of our flapping-wing aerodynamic model. We can estimate the aerodynamic forces around the flat-plate wing for the case of the lift coefficients, $J \geq 5$ and the thrust coefficients, $J \geq 3.5$.

In the near future, we will perform the next step experiments under passive and active pitching motions. It will give us the proper pitching motion to enhance the characteristics of lift and thrust. Moreover, the applicable range of our flapping-wing aerodynamic model will be reevaluated.

ACKNOWLEDGEMENT

This work was supported by the Korea Research Foundation Grant funded by the Korean Government (MOEHRD) (KRF-2007-313-D00122). The first three authors would like to thank the Brain Korea 21 Project in 2007.

REFERENCES

[1] J. D. DeLaurier, "An aerodynamic model for flapping-wing flight," *Aeronaut. J.* **97(964)**, 125-130 (1993).

[2] D.-K. Kim, J.-S. Lee, J.-Y. Lee and J.-H. Han, "An aeroelastic analysis of a flexible flapping wing using modified strip theory," *SPIE Smart Structures and Materials & Nondestructive Evaluation and Health Monitoring*, San Diego, CA, USA, Mar. 2008.

[3] S. Sunada and A. Sakaguchi, "Unsteady forces on a two-dimensional wing in plunging and pitching motions," *AIAA J.* **39(7)**, 1230-1239 (2001).

[4] M. Okamoto and A. Azuma, "Experimental study on aerodynamic characteristics of unsteady wings at low Reynolds number," *AIAA J.* **43(12)**, 2526-2536 (2005).

[5] M. J. C. Smith, P. J. Wilkin and M. H. Williams, "The advantages of an unsteady panel method in modeling the aerodynamic forces on rigid flapping wings," *J. Exp. Biol.* **199**, 1073-1083 (1996).

[6] S. A. Ansari, R. Żbikowski and K. Knowles, "Aerodynamic modeling of insect-like flapping flight for micro air vehicles," *Prog. Aerosp. Sci.* **42**, 129-172 (2006).

[7] A. J. Ward-Smith, *Biophysical Aerodynamics and the Natural Environment*, 68-122, John Wiley & Sons, 1984.